Atmos. Chem. Phys. Discuss., 15, 6445–6479, 2015
www.atmos-chem-phys-discuss.net/15/6445/2015/
doi:10.5194/acpd-15-6445-2015

Atmospheric Chemistry and Physics Discussions

Smoke aerosol properties and ageing effects for Northern temperate and boreal regions derived from AERONET source and age attribution

T. Nikonovas, P. R. J. North, and S. H. Doerr

Geography Department, College of Science, Swansea University, Singleton Park, Swansea, SA2 8PP, UK

Received: 17 December 2014 – Accepted: 11 February 2015 – Published: 5 March 2015

Correspondence to: T. Nikonovas (tadas.nik@gmail.com)

Published by Copernicus Publications on behalf of the European Geosciences Union.

Abstract

Particulate emissions from wildfires impact human health and have a large but uncertain effect on climate. Modelling schemes depend on information about emission factors, emitted particle microphysical and optical properties and ageing effects, while satellite retrieval algorithms make use of characteristic aerosol models to improve retrieval. Ground based remote sensing provides detailed aerosol characterisation, but does not contain information on source. Here, a method is presented to estimate plume origin land cover type and age for AERONET aerosol observations, employing trajectory modelling using the HYSPLIT model, and satellite active fire and aerosol optical thickness (AOT) observations from MODIS and AATSR. It is applied to AERONET stations located in or near Northern temperate and boreal forests, for the period 2002–2013. The results from 629 fire attributions indicate significant differences in size distributions and particle optical properties between different land cover types. Smallest fine mode median radius are attributed to plumes from cropland – natural vegetation mosaic (0.143 µm) and grasslands (0.147 µm) fires. Evergreen needleleaf forest emissions show a significantly smaller fine mode median radius (0.164 µm) than plumes from woody savannas (0.184 µm) and mixed forest (0.193 µm) fires. Smoke plumes are predominantly scattering for all of the classes with median single scattering albedo at 440 nm (SSA(440)) values close to 0.95 except the cropland emissions which have a SSA(440) value of 0.9. Overall fine mode volume median radius increase rate is 0.0095 µm per day for the first 4 days of ageing and 0.0084 µm per day for seven days of ageing. Changes in size were consistent with a decrease in Angstrom Exponent and increase in Asymmetry parameter. No significant changes in SSA(λ) with ageing were found. These estimates have implications for improved modelling of aerosol radiative effects, relevant to both climate modelling and satellite aerosol retrieval schemes.

ACPD
15, 6445–6479, 2015

1 Introduction

Vegetation fires are estimated to emit ~ 2.0 Pg of carbon per year into the atmosphere (van der Werf et al., 2010) influencing air quality, weather and climate (Bevan et al., 2009; Langmann et al., 2009). Particulate matter emissions adversely affect human health and mortality rates (Johnston et al., 2012), and have a substantial but very uncertain effect on the Earth's radiative budget (Bond et al., 2013). Climate model intercomparison (Myhre et al., 2013) indicates little agreement in simulated magnitude and sign of direct radiative forcing attributed to biomass burning emissions. Smoke plumes are difficult to observe, characterise and represent in climate models because they contain chemically and microphysically complex particles that evolve during their atmospheric lifetimes. Improving the characterisation of emission factors, aerosol optical properties, mixing effects and microphysical processes in modelling schemes were identified as key directions narrowing the uncertainties and reducing model and observational biases (Koch et al., 2009; Bauer et al., 2010; Bond et al., 2013).

Characterisation of smoke aerosols is a fundamentally difficult problem because of the dynamic nature of combustion particle formation and evolution. Particulate emission from open biomass burning consists primarily of scattering organic matter and soot – agglomerates of carbon nanospheres (Buseck et al., 2012) which are strong absorbers and have a significant warming effect (Bond et al., 2013). Soot structures are not discretely separate, but are embedded in, or have organic coatings (Reid et al., 2005a). Smoke particle size distributions are typically bimodal with the bulk of mass concentrated in the fine mode (aerosols 0.1 to 1 µm in diameter). The proportions of different chemical species, particle size distributions, mixing state and hence optical properties of the particles vary greatly depending on the fuel type and moisture, combustion phase, fire intensity and meteorological conditions at the time of emission (Reid et al., 2005a, b; Janhäll et al., 2010, and references therein).

Smoke emitted from different vegetation types indicate distinctiveness in particle size distributions and optical properties. Emissions from Northern temperate and boreal for-

ACPD
15, 6445–6479, 2015

est fires are generally less absorbing and tend to have larger particles than Amazonian or African forest burn plumes (Hobbs et al., 1996; Dubovik et al., 2002; Eck et al., 2003), due to differences in fuels, combustion phase and fire intensity (Reid et al., 2005a). Flaming fires are generally thought to emit larger and more absorbing particles (Hobbs et al., 1996; Reid and Hobbs, 1998; Janhäll et al., 2010). However, there is evidence that strongly smouldering combustion of peat fuels in particular can generate even larger particles (Nakajima et al., 1999; Eck et al., 2003).

The complexity of the parametrisation increases with ageing processes. Emitted smoke particles are lofted to altitudes ranging from hundreds to thousands of meters, frequently above the planetary boundary layer (Kahn et al., 2008; Martin et al., 2010), and in some cases to the lower stratosphere (Damoah et al., 2006). During the lifetime of several days to weeks plumes can be transported on regional (Colarco et al., 2004) or intercontinental (Damoah et al., 2004; Dirksen et al., 2009) scales. Ageing aerosols undergo chemical and physical transformations. Measured increases in particle size have been attributed to coagulation (Reid et al., 1998; Fiebig et al., 2003; Colarco et al., 2004), condensation (Cocker et al., 2001; Carrico et al., 2005) and coating (Dahlkötter et al., 2013). The exact effects of these processes on the radiance field are not established and only recently has ageing been introduced into modelling schemes (Bauer et al., 2010). An increasing number of studies indicate the impact of aerosol mixing state and morphology (Bauer et al., 2010; Shiraiwa et al., 2010; Cappa et al., 2012) on optical properties stressing the need to parameterise these processes in models. A ratio of scattering extinction to total extinction, single scattering albedo (SSA(λ)), has been reported to increase in ageing plumes (Reid and Hobbs, 1998; O'Neill et al., 2002; Abel et al., 2003; Eck et al., 2009) indicating greater enhancement in scattering efficiency compared to absorption. In addition, laboratory based experiments (Shiraiwa et al., 2010) and modelling studies (Jacobson, 2001; Bauer et al., 2010) suggest a significant increase in absorption in ageing smoke due to the lensing effect, where by the thickening coating of scattering matter increases particle optical cross-section and

ACPD
15, 6445–6479, 2015

redirects more radiation towards the absorbing core. Ambient aerosol measurements (Cappa et al., 2012), however, indicate only modest absorption enhancement.

Observation and retrieval of smoke optical parameters by remote sensing is challenging because of particularly high spatial and temporal variability in plume occurrence and evolution. Satellite remote sensing provides global and continuous measurements of Aerosol Optical Thickness (AOT) with improving accuracy and between-sensor agreement (Kinne et al., 2003; Kokhanovsky et al., 2010; de Leeuw et al., 2013; Holzer-Popp et al., 2013). However, while methods based on UV absorption, or multi-angle retrieval offer potential to resolve further aerosol properties, (Torres et al., 2007; Kahn et al., 2009; Dubovik et al., 2011), the presence of variable background reflectance over land surfaces makes routine operational retrieval of aerosol absorption problematic, especially at low optical thickness. Accordingly, many retrieval schemes make use of a priori knowledge of properties of characteristic aerosol types within retrievals.

Ground based Aerosol Robotic Network (AERONET) sun and sky photometers (Holben et al., 1998) located at locations worldwide, provide more robust aerosol measurements. The observations are less affected by the surface reflectance component and are not limited to one or a few view angles. Retrieved aerosol optical and physical properties are fundamental in determining dominant aerosol types for various regions (Dubovik et al., 2002; Lee et al., 2010; Giles et al., 2012) and have become a benchmark for validating satellite observations (Kokhanovsky et al., 2010; Holzer-Popp et al., 2013). AERONET aerosol characterisations have been derived by taking average values from a set of stations assumed to be representative to a certain region or aerosol type. This approach approximates complexities and variability in aerosol properties, but it does not exploit some of the information contained in individual AERONET observations. For example a record from stations located at or near boreal forest is likely to include observations of smoke of various age and origin. Several studies used atmospheric transport modelling and satellite data to determine the source and age for a set of AERONET smoke observations, focusing on individual burning events (O'Neill et al.,

ACPD
15, 6445–6479, 2015

2002; Eck et al., 2009; Dahlkötter et al., 2013). Sayer et al. (2014) subdivided sets of AERONET stations representing biomass burning regions into near source and distant ones to explore the ageing effects on optical and microphysical properties. These studies stress the need for smoke plume source and age resolved analysis methods establishing particle properties for different emission sources and long term ageing effects.

This study addresses this research gap by improving the characterisation and ageing effects of smoke plumes typically attributed to Northern temperate and boreal forests. A new method is presented here allowing the estimation of age and source for AERONET aerosol observations. The method is applied with a focus on two aims. The first is to determine smoke particle microphysical and optical properties for emissions from different vegetation types. Explicit source attribution offers additional information content compared to region-based approaches (Dubovik et al., 2002; Giles et al., 2012; Sayer et al., 2014) and could partly address the large variability in aerosol properties characteristic to the boreal forests. The second aim is to explore changes in particle properties occurring in plumes over several days of ageing, complementing existing studies (Reid et al., 1998; Capes et al., 2008; Eck et al., 2009) with independent estimates based on an alternative method and larger sample.

2 Data and methods

The source and age estimation for AERONET smoke observations was achieved by using an air parcel trajectory model and satellite active fire and AOT observations. For all of the selected AERONET smoke observations described in Sects. 2.1 and 2.1.1, a set of air parcel back trajectories ending at a range of altitudes was generated using the HYSPLIT model as specified in Sect. 2.3. Coinciding satellite active fire (Sect. 2.2) and AOT observations (Sect. 2.4) along the trajectories were used as inputs into the decision tree outlined in Sect. 2.5 and Fig. 4, estimating source and age for the AERONET observations.

ACPD
15, 6445–6479, 2015

2.1 AERONET data

The analysis is based on AERONET Level 2.0 version 2 inversion data products. AERONET CIMEL radiometers are calibrated and continuously monitored, and data products are cloud screened and undergo robust standardised processing (Holben et al., 2006) which enables quantitative comparative analysis. Direct solar extinction measurements provide columnar AOT at several wavelengths ranging from 340 to 1640 nm. Combined direct sun and diffuse sky radiance measurements at four wavelengths (440, 676, 879 and 1020 nm) are best-fitted with radiative transfer model effectively retrieving columnar aerosol size distribution, spectral complex refractive index, SSA(λ), Angstrom Exponent (AE), Absorption Angstrom Exponent (AAE), phase function and precipitable water content (Dubovik and King, 2000; Dubovik et al., 2006). Retrieved aerosol optical properties and size distributions are in agreement with independent in-situ aerosol measurements (Haywood et al., 2003; Johnson et al., 2009) and have well defined uncertainties (Dubovik et al., 2000; Holben et al., 2006). The accuracy is improved during higher aerosol loading conditions and therefore AERONET level 2 inversion products contain only retrievals at AOT(440) levels of 0.4 or higher. Size distribution parameters and optical properties discussed throughout this study are consistent with the definitions and units described in Holben et al. (2006).

2.1.1 Data selection

This study uses data from AERONET stations positioned within or in proximity to the Northern boreal and temperate forests. All available level 2 data from the stations located north of 45° latitude in North America and Asia (Fig. 1) and collected at any time from the year 2002 through 2013 were selected. European observations were excluded because of higher background AOT levels and more likely mixing of smoke plumes with urban and industrial aerosol. Temporal extent of the study was constrained by the start date of MODIS data availability from both platforms Terra and Aqua in early 2002. AOT record from the selected AERONET stations indicate generally low aerosol background

ACPD
15, 6445–6479, 2015

levels with sharp spikes in aerosol loading occurring during the burning season lasting from late spring to early autumn. The pattern suggests that the majority of level 2 retrievals (AOT(440) > 0.4) is a record of biomass burning plumes. Notably, this study is not fully inclusive or exclusive to the Northern forest emissions both in terms of vegetation type or geographic extent. Plumes transported to the selected AERONET locations from areas extending beyond the region of interest and attributed to a range of land cover types have been included in the analysis.

Severe burning seasons in 2004 and 2005 in Alaska caused very high AOT(λ) values ~ (2–5) recorded at Bonanza Creek AERONET station. The very large (0.2–0.25) fine mode volume median radius (R_{fv}) values retrieved during these events were attributed to peat fuel combustion (Eck et al., 2009). The method used in this study could not establish ageing properties for these plumes because of large number of active fires and persistently elevated AOT levels in the region. As a result Bonanza Creek observations for August in years 2004 and 2005 have been excluded from the analysis.

2.2 Active fire data

As a proxy for fire activity during the period analysed, the MODIS fire location dataset MCD14ML produced by the University of Maryland and provided by NASA Fire Information for Resource Management System was used. The dataset contains active fire detections from Terra and Aqua platforms with information of the hot spot location, brightness temperature at MODIS bands 21 and 31, fire radiative power and detection confidence (Giglio et al., 2003).

2.2.1 Fire data processing and selection

Fire inventories compiled for Alaska (Stocks et al., 2002) and Canada (Kasischke et al., 2002) indicate that very large fires are not numerous, but account for the majority of the total area burned. Stocks et al. (2002) found that fires larger than 100 km^2 represented more than 80 % of total area burned. Following this only large wildfire events likely to be

ACPD
15, 6445–6479, 2015

strong emission sources were considered in the analysis. To identify such fires MODIS individual hot spots with 80 % or more detection confidence were agglomerated into fire events using the Density Based Spatial Clustering (DBSCAN) algorithm (Ester et al., 1996). DBSCAN clustering was performed merging individual fire detections into a single fire object if at least two were found closer together than 10 km in space and 24 h in time. The objects were iteratively formed by adding any fire points found within the search radius from all of the fire detections belonging to the cluster (Fig. 2). Identified fire events were considered as large and selected for the analysis if the event duration was more than 48 h, and the spatial bounding box including all points belonging to the event was larger than 100 km^2.

2.2.2 Fire and emission source land cover type

The emission source land cover type for each of the fire events was determined using MODIS MCD12C1 annual land cover type data products which employ 17 different land cover classes defined by the International Geosphere Biosphere Programme (Loveland and Belward, 1997). Initially, the land cover type was identified for each of the active fire pixels within a fire event from a grid value given in the MCD12C1 product from a corresponding year. The land cover value occurring most often (mode) was used as a land cover type identifier for the fire event. This was done for all of the years except 2013 for which MCD12C1 is unavailable and the 2012 product was used instead.

2.3 Back trajectories

To link AERONET observations with source regions and to identify the likely smoke transport pathways, air mass trajectories were computed with HYSPLIT (Hybrid Single-Particle Lagrangian Integrated) model (Draxler and Rolph, 2003). The HYSPLIT model was run using Global Data Assimilation System (GDAS) meteorological archive data for the available 2005–2013 period and NCEP/NCAR reanalysis data for 2002–2004. For each of the studied AERONET elevated AOT observations (AOT at 440 nm above 0.4)

ACPD
15, 6445–6479, 2015

seven day back trajectories with one hour temporal step were generated starting at 16 elevations ranging from 500 to 12 000 m: at 500 m intervals below 4000 and at 1000 m intervals above 4000 m. The uncertainty in the individual trajectories was assessed, estimating HYSPLIT Model numerical integration and meteorological data resolution errors. The first was estimated computing back trajectory and then forward trajectory from the back trajectory's end point. The error was assumed to be half of the horizontal and vertical distance between the initial start and the final end points. The resolution error and resultant divergence in flow field was determined generating a grid of 27 ($3 \times 3 \times 3$) back trajectories beginning around the initial start point, with horizontal and vertical offsets given by the estimated numerical error.

2.4 Satellite AOT

The two independent satellite AOT data products used are based on observations from (1) The Moderate Resolution Imaging Spectrometer (MODIS) sensors on-board Terra and Aqua platforms and (2) Along Track Scanning Radiometer (AATSR) sensors flown in succession on ERS-2 and ENVISAT spacecrafts. While the method can readily be extended to include further satellite data, the role here is to confirm model tracking of plume transport from source to AERONET, rather than to add additional information on aerosol properties. The MODIS dataset M*D04_L2 is based on the dark target retrieval scheme (Kaufman and Tanre, 1998b; Levy et al., 2009) and AATSR_SU on the algorithm developed at Swansea University (North, 2002; Bevan et al., 2012), modified under the ESA Aerosol Climate Change Initiative (CCI) (Holzer-Popp et al., 2013; de Leeuw et al., 2013). Both data products provide interpolated AOT at 550 nm and have 10 km × 10 km spatial resolution. The MODIS dataset has greater spatial coverage and temporal resolution because of wider swath and two sensors operational at the same time. Importantly, both algorithms perform well compared to AERONET AOT observations. Validation studies suggest RMSE from 0.1 to 0.2, and little bias between AERONET and both satellite AOT retrieval schemes (Levy et al., 2010; Holzer-Popp et al., 2013). It must be noted that the assessments and RMSE as a measures them-

ACPD
15, 6445–6479, 2015

selves are biased towards low AOT conditions, which constitute the vast majority of the observations. Discrepancies can be expected to be larger for the aerosol loadings (AOT(440) > 0.4) analysed herein. However, the accuracy of satellite AOT observations was not critical for the purpose of this study.

2.5 Age and source estimation

Smoke source attribution for AERONET observations was performed by finding coinciding satellite AOT and fire event observations along the generated trajectories and identifying candidate plume pathways. Starting at an AERONET station and an observation time, for each trajectory level spatiotemporal queries were performed, finding any satellite AOT and fire event observations falling within the trajectory domains at hourly steps (Fig. 3). The location and size of spatial search windows at each time step was given by the trajectory uncertainty analysis. Identified AOT observations and proximity to large fire events served as inputs into the decision tree. A trajectory was selected as a candidate if the conditions showed in Fig. 4 were satisfied. When several candidate trajectories were selected, the trajectories were ranked according to the potential fire source size and satellite AOT values observed after the trajectory has passed the source. Finally, the highest ranked candidate was identified as the source and age estimate.

2.6 Statistical methods

A linear regression was used to examine ageing effects on smoke particle microphysical and optical properties. Both positive or negative correlation between the age estimates and a particular property was considered significant if two-sided p value was ≤ 0.01. Error estimates and uncertainty intervals stated represent 95 % confidence intervals in regression coefficients.

ACPD
15, 6445–6479, 2015

The differences in properties of plumes attributed to different land cover types were assessed by the Mann-Whitney U test. Two samples are identified as significantly different if the two-sided p value was ≤ 0.01.

3 Results and discussion

From a total of 1337 AERONET observations processed, age and source were determined for 629. The majority of the identifications are for smoke of up to 1–2 days of age, and the counts are increasingly smaller for older estimates (Fig. 1c). Due to a small number of identified observations of plumes aged more than 4 days, the results are more robust when considering the first 4 days of ageing. This is an expected outcome because it is progressively less likely that the plume evolution is tracked successfully, satisfying all of the decision tree conditions, as smoke ages. Inclusion of European AERONET observations could potentially increase the numbers for old smoke as many aged North American and, to a lesser extent, Asian boreal forest plumes are observed in Europe (Damoah et al., 2004; Dahlkötter et al., 2013). However, the method currently does not perform well in the cases of extremely long transport and high background AOT levels, and thus the number of additional estimates would be small.

3.1 Emission source

The most frequent emission source land cover type determined was evergreen needleleaf forest (ENF) constituting more than half of all estimates (Fig. 1b). The dominance could indicate exceptional fire activity or emission characteristics resulting in significantly more plumes originating in ENF compared to other land cover types. However, we suggest that it is likely to be merely a consequence of ENF spatial distribution and location of the AERONET stations used in the analysis. ENF occupies large areas stretching from North to South in Western Canada and USA with many AERONET stations located to the East. Smoke dispersion towards the stations is accommodated by

ACPD
15, 6445–6479, 2015

prevailing East–West transport at these latitudes. It is important to consider sample size inconsistencies when evaluating the variability in particle properties between plumes attributed to different land cover types. Distributions for classes with a small number of estimates exhibit multimodality (Fig. 5) and thus their summary metrics should be treated with caution.

Particle size distributions derived for the source land cover type classes indicate distinctiveness in fine mode volume median radius (R_{fv}). Cropland/natural vegetation mosaic and grassland emissions tend to show the smallest particles, with median R_{fv} values 0.143 and 0.147 µm. Plumes from mixed forests generally contain the largest particles followed by wooded savannas having median R_{fv} values 0.193 and 0.186 µm respectively. The most numerous ENF smoke observations typically have particles smaller than the emissions from mixed forests and woody savannas, with determined median R_{fv} 0.164 µm.

These estimates generally agree with published size distributions for various fuel types. Grass fires are reported to emit smaller particles (Reid and Hobbs, 1998) than forest fires (Dubovik et al., 2002). Plumes with the smallest median R_{fv} in this study are attributed to grass, cropland/natural vegetation mosaic and ENF fires. This could be because of smaller fire intensities in these cover types compared to fires in mixed forest and wooded savannas (Reid et al., 2005a). As well as differences in burning intensity, large particles in the later classes could be influenced by the presence of significant amounts of peat in these biomes, the combustion of which is known to generate very large particles (Eck et al., 2009).

The distinctiveness in particle size distributions attributed to the three forest cover types – ENF, mixed forests and wooded savannas – is particularly interesting. It indicates significant differences in fuels, combustion conditions and fire intensities between these vegetation types which are typically agglomerated under broad boreal forest definition. Boreal smoke size distributions are known to have generally larger R_{fv} compared to African or Amazon forest emissions (Reid et al., 2005a), but are also reported to exhibit high variability in retrieved properties (Eck et al., 2003, 2009). The results

ACPD
15, 6445–6479, 2015

obtained in this study indicate that some of the variability could be addressed by the source attribution.

The differences in optical properties between plumes attributed to the land cover classes considered are more subtle. The variability in single scattering albedo and its spectral dependence is small. Inferred median SSA(440) is within the AERONET uncertainty interval of 0.02 from an 0.95 value for all land covers except for the plumes from cropland/natural vegetation mosaic fires, which are more absorbing and have a median SSA(440) value of 0.9. Notably, in this land cover class the lowest SSA(440) corresponds both to the smallest median R_{fv} and to the highest median imaginary part of the refractive index (Fig. 7a, d and b). Smoke from mixed forests, with a median SSA(440) value of 0.963, is slightly less absorbing than ENF and wooded savannas emissions which both have median SSA(440) values of 0.95. These differences in absorption magnitude suggest some variability in flaming vs. smouldering combustion ratios and is consistent with observed differences in size distributions. However, there is little to differentiate between the different forest types considered here based solely on optical properties. The often reported SSA(λ) values close to 0.95 for boreal regions (Dubovik et al., 2002; Reid et al., 2005b) seems to be applicable for emissions from all forest types discussed here.

3.2 Particle growth rates

There is a significant relationship between the age estimates and AERONET retrieved smoke particle size distributions. Figure 6a shows AERONET retrieved fine mode volume median radius (R_{fv}) plotted against the age estimates. A linear fit suggests a R_{fv} growth rate of 0.0084 µm (0.0072–0.0098 µm CI) per day. Published smoke particle growth rates vary and are difficult to compare due to differences in measuring techniques, sampled fuels, fire size, intensity, combustion phase and smoke age. Reid et al. (2005a) concluded in their review that, on average, aged smoke particle distributions have R_{fv} larger by 0.025 µm. In agreement with this, the growth rate derived in this study indicates an increase in R_{fv} of 0.025 µm in approximately 3 days.

ACPD
15, 6445–6479, 2015

The SD from R_{fv} does not exhibit significant dependence on estimated age. Generally, distributions with smaller R_{fv} tend to have a smaller spread (Fig. 6d). The relationship between R_{fv} and R_{fv} spread is stronger for young smoke and is not evident for the aged smoke observations. This indicates that while particle sizes increase in ageing plumes, the spread of the fine mode volume radius does not change systematically.

The age and R_{fv} relationships seen in Fig. 6a exhibit a degree of non-linearity. Quadratic fit indicates initially faster and gradually decreasing growth rates. Due to the small number of very old smoke observations it is not possible to determine whether the non-linearity is significant. However, the data available suggests that there is a change in the R_{fv} increase trend after 3–4 days of ageing. Notably, a linear fit on the selected data subset of observations up to 4 days old indicates a higher aerosol growth rate of 0.0095 µm (0.0069–0.012 µm CI) per day. In that case 0.025 µm in R_{fv} is gained in between 2 and 3 days. The inferred gradual slow down in growth integrates well with the reported stabilisation in size distributions in Brazilian smoke after 3 days of ageing (Kaufman et al., 1998a; Reid et al., 1998). These studies suggest the increase in size is due to coupled coagulation and condensation processes during the first 1–4 days followed by predominantly coagulation growth afterwards.

The derived linear model coefficients are significant but the spread of the values is large. The high variability can be partly explained by significant differences in size distributions between plumes attributed to different land cover sources. The growth rates derived for smoke of different origin seen in Fig. 7a are notably similar despite varying sample sizes. All estimates fall within the confidence interval of the regression slope for all of the data with the exception of ENF plumes for which the derived growth rate is slightly lower.

Variances in particle R_{fv} within the fire source classes are nonetheless large. This could be due to any of the following factors: (1) erroneous age and source attribution in the case of mixture of fresh smoke and aged regional haze or mixture with different aerosol species; (2) inevitably large intra-class variability in a range of factors determining particle sizes during the combustion; (3) fast processes beyond the temporal

ACPD
15, 6445–6479, 2015

resolution of the proposed method and data. A number of studies have measured very rapid dynamics including significant particle growth during the first few hours of ageing (Hobbs et al., 1996; Abel et al., 2003; Calvo et al., 2010). Growth rates can be particularly high in concentrated plumes with high aerosol loading due to more frequent collisions between particles, fast condensation (water and organics) and gas to particle conversion. The AERONET records typically do not include observations of truly fresh smoke within seconds or minutes after the emission. As a result of this limitation and the uncertainty originating from the age estimation method employed in this study, the analysis has only a moderate temporal resolution and is limited to relatively long term ageing processes. Figure 6a indicates that fresh smoke observations with largest retrieved R_{fv} tend to have higher AOT values and wider R_{fv} spread. Assuming that the age and source estimates are correct for these cases, the explanation may be unusual fuel and combustion characteristics or fast particle growth at high aerosol concentrations.

3.3 Changes in precipitable water content

There is a significant correlation between AERONET retrieved columnar precipitable water content and the age estimates (Fig. 7c). Generally, older plumes tend to be mixed in air masses with higher water content. The relationship is similar to R_{fv} ageing pattern, but suggests an even higher degree of non-linearity. The quadratic fit exhibits a peak in AERONET precipitable water content at around 3–4 days of ageing and a subsequent decrease. This pattern suggests that, when plumes are being transported further from sources, they are entrained within progressively more moist air masses. A relationship between water vapour content and AOT has been observed (Hegg et al., 1997; Smirnov et al., 2000), indicating that it is one of the main contributors to total AOT. The results presented in this study show that plumes from mixed forest and open shrubland land cover classes tend to be transported within air masses with higher water vapour content. Notably, the same plumes tend to have larger particles and higher growth rates. This may suggest that water condensation plays a role in inferred particle growth during the first few days of ageing, complementing reported transition from condensa-

ACPD
15, 6445–6479, 2015

tion and coagulation growth to coagulation growth after 3–4 days of ageing (Kaufman et al., 1998a; Reid et al., 1998).

3.4 Changes in optical properties

In contrast to particle size distributions, the SSA(λ) and age relationship is not statistically significant and falls within the uncertainty interval of 0.02 for individual AERONET SSA(λ) retrievals (Fig. 7e). Mie theory predicts that particle radius growth due to coagulation should generally result in smaller absorption and higher scattering efficiency, hence an increase in SSA(λ) (Bond and Bergstrom, 2006). Such an increase in ageing smoke has been observed in Brazil (Reid et al., 1998), West Africa (Abel et al., 2003; Capes et al., 2008), Spain (Calvo et al., 2010) and North America (Eck et al., 2009). Notably, most of the aforementioned studies were analysing inherently more absorbing smoke with typically smaller particles compared to emissions from the sources explored in this study. It is possible that most of the scattering enhancement happens during the rapid evolution phase within few hours from the emission and thus can not be observed by the method employed in this study.

There is a significant tendency for the absorption angstrom exponent (AAE) to decrease at a rate of −0.034 (−0.014 to 0.054 CI) per day with age, suggesting some changes in chemical composition in the ageing plumes (Fig. 7d). The significance of condensation of organics as well as water vapour in aerosol growth is well established (Reid et al., 2005b; Dahlkötter et al., 2013). The effects of these processes on optical properties are less clear (Bond and Bergstrom, 2006; Cappa et al., 2012). Enhancements in wavelength dependent absorption due to increasing organic carbon content should result in higher absorption angstrom exponent values. However, the results imply a decrease in AAE in ageing plumes.

The angstrom exponent (AE) decreases with age (Fig. 7c) at a rate of −0.05 (−0.038 to −0.063 CI) per day considering all land cover types. Decreasing wavelength dependence of AOT corresponds to inferred particle growth and is an expected result. Similarly, the asymmetry parameter tends to increase in ageing plumes (Fig. 7f) indicating

ACPD
15, 6445–6479, 2015

increasing back-scatter due to growth in R_{fv}. There are, however, some notable differences between the land cover types. Estimated change rates in the asymmetry parameter and AE vary by a factor of two or more. Although they largely agree, changes in AE and the asymmetry parameter do not mirror inferred particle growth rates exactly. This variability could be due to uncertainties in AERONET inversions, insufficient sample size for some land cover classes, or they could reflect effects of differences in particle chemistry affecting AE and the asymmetry parameter besides particle size.

There is a significant negative correlation between AOT(440) and estimated plume age (Fig. 7g). AOT(440) values decline at a rate of −0.048 (−0.024 to −0.072 CI) per day considering all observations. The AOT(λ) and estimated age relationship is not significant for longer wavelengths. This suggests that a positive correlation between particle size and AOT (Reid et al., 1998; Sayer et al., 2014) is counteracted by the reduction in particle concentrations in ageing plumes.

4 Conclusions

This study presents an analysis of ageing effects on smoke particle size distribution and optical properties in regions associated with large variability in aerosol characteristics. A new method was developed allowing the source and age attribution for AERONET aerosol observations, and applied to data from stations located in or near Northern temperate and boreal forests in North America and Asia.

The results show that plume properties vary with the determined source vegetation type as defined by the land cover classification scheme. Notable variability exists not only when comparing emissions from grasslands, croplands and forests, but also different forest types. Plumes from mixed forests generally contain the largest particles with a median R_{fv} 0.193 µm, followed by emissions from wooded savannas and shrubland. Smoke attributed to evergreen needleleaf forest fires exhibit smaller particles than other forest emissions, having median R_{fv} value 0.164 µm which is close to the R_{fv} values of 0.143 and 0.147 µm observed in plumes from cropland and grass fires. Estimated me-

ACPD
15, 6445–6479, 2015

dian SSA(440) values range from 0.95 to 0.97 for all of the sources considered in this study with the notable exception of cropland and natural vegetation plumes which are substantially more absorbing with SSA(440) value of 0.9.

Derived particle R_{fv} growth rates are 0.0095 µm (0.0069–0.012 µm confidence interval) per day for the first 4 days and 0.0084 µm (0.0072–0.0098 µm) per day for 7 days of ageing. These independent estimates are based on a large sample, compare favourably with existing estimates and refine growth rates obtained by different methods. The particle growth rates derived for plumes from different vegetation types are remarkably similar, implying comparable processes driving the growth. Inferred slow down in growth rates at around 3–4 days of ageing has been observed before (Kaufman et al., 1998a; Reid et al., 1998) and suggests a shift in particle growth processes.

A significant relationship is observed between AERONET columnar precipitable water content and estimated age. It suggests that ageing plumes are entrained in air masses with higher water content. Particle growth rates are higher for smoke which is transported within air masses containing more precipitable water, implying higher contribution of hygroscopic growth.

In contrast to size distributions, smoke SSA(λ) do not exhibit strong dependence on age. The inferred changes in SSA(λ) are not significant and do not exceed AERONET uncertainty bounds. The angstrom exponent is decreasing while the asymmetry parameter is increasing with age, reflecting the increase in particle R_{fv}. The absorption angstrom exponent tends to decrease with age.

The method and results presented here allow the microphysical and optical characterisation of particulate emissions from different vegetation types to be improved. Estimated ageing effects provide information on long term particle evolution and active processes that can be used in parameterising and validating modelling schemes and improving aerosol models used by satellite retrieval algorithms.

Acknowledgements. This study was supported by the Natural Environment Research Council (NERC). The authors gratefully acknowledge the AERONET team for their effort in establishing and maintaining the network, and the data provision. NOAA Air Resources Laboratory (ARL) for

ACPD
15, 6445–6479, 2015

the provision of the HYSPLIT transport and dispersion model. MODIS collection 5.1 M*D05_L2 datasets were obtained from the Level 1 and Atmosphere Archive and Distribution System (LAADS) FTP site. Fire Information for Resource Management System (FIRMS) MODIS fire hotspot data was obtained from the NASA Earth Observing System Data and Information System (EOSDIS) site. MODIS MCD12C1 land cover type data was downloaded from the Land Processes Distributed Active Archive Center (LP DAAC) site. AATSR_SU version 4.2 datasets were made available under the ESA Aerosol CCI project http://www.esa-aerosol-cci.org.

References

Abel, S. J., Haywood, J. M., Highwood, E. J., Li, J., and Buseck, P. R.: Evolution of biomass burning aerosol properties from an agricultural fire in southern Africa, Geophys. Res. Lett., 30, 1783, doi:10.1029/2003GL017342, 2003. 6448, 6460, 6461

Bauer, S. E., Menon, S., Koch, D., Bond, T. C., and Tsigaridis, K.: A global modeling study on carbonaceous aerosol microphysical characteristics and radiative effects, Atmos. Chem. Phys., 10, 7439–7456, doi:10.5194/acp-10-7439-2010, 2010. 6447, 6448

Bevan, S. L., North, P. R., Grey, W. M., Los, S. O., and Plummer, S. E.: Impact of atmospheric aerosol from biomass burning on Amazon dry-season drought, J. Geophys. Res.-Atmos., 114, D09204, doi:10.1029/2008JD011112, 2009. 6447

Bevan, S. L., North, P. R., Los, S. O., and Grey, W. M.: A global dataset of atmospheric aerosol optical depth and surface reflectance from AATSR, Remote Sens. Environ., 116, 199–210, 2012. 6454

Bond, T. C. and Bergstrom, R. W.: Light absorption by carbonaceous particles: an investigative review, Aerosol Sci. Tech., 40, 27–67, 2006. 6461

Bond, T. C., Doherty, S. J., Fahey, D. W., Forster, P. M., Berntsen, T., DeAngelo, B. J., Flanner, M. G., Ghan, S., Kärcher, B., Koch, D., Kinne, S., Kondo, Y., Quinn, P. K., Sarofim, M. C., Schultz, M. G., Schulz, M., Venkataraman, C., Zhang, H., Zhang, S., Bellouin, N., Guttikunda, S. K., Hopke, P. K., Jacobson, M. Z., Kaiser, J. W., Klimont, Z., Lohmann, U., Schwarz, J. P., Shindell, D., Storelvmo, T., Warren, S. G., and Zender, C. S.: Bounding the role of black carbon in the climate system: a scientific assessment, J. Geophys. Res.-Atmos. 118, 5380–5552, doi:10.1002/jgrd.50171, 2013. 6447

ACPD
15, 6445–6479, 2015

Buseck, P. R., Adachi, K., Gelencsér, A., Tompa, É., and Pósfai, M.: Are black carbon and soot the same?, Atmos. Chem. Phys. Discuss., 12, 24821–24846, doi:10.5194/acpd-12-24821-2012, 2012. 6447

Calvo, A., Pont, V., Castro, A., Mallet, M., Palencia, C., Roger, J., Dubuisson, P., and Fraile, R.: Radiative forcing of haze during a forest fire in Spain, J. Geophys. Res.-Atmos., 115, D08206, doi:10.1029/2009JD012172, 2010. 6460, 6461

Capes, G., Johnson, B., McFiggans, G., Williams, P., Haywood, J., and Coe, H.: Aging of biomass burning aerosols over West Africa: aircraft measurements of chemical composition, microphysical properties, and emission ratios, J. Geophys. Res.-Atmos., 113, D00C15, doi:10.1029/2008JD009845, 2008. 6450, 6461

Cappa, C. D., Onasch, T. B., Massoli, P., Worsnop, D. R., Bates, T. S., Cross, E. S., Davidovits, P., Hakala, J., Hayden, K. L., Jobson, B. T., Kolesar, K. R., Lack, D. A., Lerner, B. M., Li, S.-M., Mellon, D., Nuaaman, I., Olfert, J. S., Petäjä, T., Quinn, P. K., Song, C., Subramanian, R., Williams, E. J., and Zaveri, R. A.: Radiative absorption enhancements due to the mixing state of atmospheric black carbon, Science, 337, 1078–1081, 2012. 6448, 6449, 6461

Carrico, C. M., Kreidenweis, S. M., Malm, W. C., Day, D. E., Lee, T., Carrillo, J., McMeeking, G. R., and Collett Jr, J. L.: Hygroscopic growth behavior of a carbon-dominated aerosol in Yosemite National Park, Atmos. Environ., 39, 1393–1404, 2005. 6448

Cocker, D. R., Whitlock, N. E., Flagan, R. C., and Seinfeld, J. H.: Hygroscopic properties of Pasadena, California aerosol, Aerosol Sci. Tech., 35, 637–647, 2001. 6448

Colarco, P., Schoeberl, M., Doddridge, B., Marufu, L., Torres, O., and Welton, E.: Transport of smoke from Canadian forest fires to the surface near Washington, DC: injection height, entrainment, and optical properties, J. Geophys. Res.-Atmos., 109, D06203, doi:10.1029/2003JD004248, 2004. 6448

Dahlkötter, F., Gysel, M., Sauer, D., Minikin, A., Baumann, R., Seifert, P., Ansmann, A., Fromm, M., Voigt, C., and Weinzierl, B.: The Pagami Creek smoke plume after long-range transport to the upper troposphere over Europe – aerosol properties and black carbon mixing state, Atmos. Chem. Phys., 14, 6111–6137, doi:10.5194/acp-14-6111-2014, 2014. 6448, 6450, 6456, 6461

Damoah, R., Spichtinger, N., Forster, C., James, P., Mattis, I., Wandinger, U., Beirle, S., Wagner, T., and Stohl, A.: Around the world in 17 days - hemispheric-scale transport of forest fire

ACPD
15, 6445–6479, 2015

smoke from Russia in May 2003, Atmos. Chem. Phys., 4, 1311–1321, doi:10.5194/acp-4-1311-2004, 2004. 6448, 6456

Damoah, R., Spichtinger, N., Servranckx, R., Fromm, M., Eloranta, E. W., Razenkov, I. A., James, P., Shulski, M., Forster, C., and Stohl, A.: A case study of pyro-convection using transport model and remote sensing data, Atmos. Chem. Phys., 6, 173–185, doi:10.5194/acp-6-173-2006, 2006. 6448

de Leeuw, G., Holzer-Popp, T., Bevan, S., Davies, W., Descloitres, J., Grainger, R. G., Griesfeller, J., Heckel, A., Kinne, S., Klüser, L., Kolmonen, P., Litvinov, P., Martynenko, D., North, P. J. R., Ovigneur, B., Pascal, N., Poulsen, C., Ramon, D., Schulz, M., Siddans, R., Sogacheva, L., Tanré, D., Thomas, G. E., Virtanen, T. H., von Hoyningen Huene, W., Vountas, M., and Pinnock, S.: Evaluation of sevenEuropean aerosol optical depth retrieval algorithms for climate analysis, Remote Sens. Environ., doi:10.1016/j.rse.2013.04.023, in press, 2013. 6449, 6454

Dirksen, R. J., Folkert Boersma, K., De Laat, J., Stammes, P., Van Der Werf, G. R., Val Martin, M., and Kelder, H. M.: An aerosol boomerang: rapid around-the-world transport of smoke from the December 2006 Australian forest fires observed from space, J. Geophys. Res.-Atmos., 114, D21201, doi:10.1029/2009JD012360, 2009. 6448

Draxler, R. and Rolph, G.: HYSPLIT (HYbrid Single-Particle Lagrangian Integrated Trajectory) model access via NOAA ARL READY website, available at: http://www.arl.noaa.gov/ready/hysplit4.html (last access: 17 December 2014), NOAA Air Resources Laboratory, Silver Spring, 2003. 6453

Dubovik, O. and King, M. D.: A flexible inversion algorithm for retrieval of aerosol optical properties from Sun and sky radiance measurements, J. Geophys. Res.-Atmos., 105, 20673–20696, 2000. 6451

Dubovik, O., Smirnov, A., Holben, B., King, M., Kaufman, Y., Eck, T., and Slutsker, I.: Accuracy assessments of aerosol optical properties retrieved from Aerosol Robotic Network (AERONET) Sun and sky radiance measurements, J. Geophys. Res.-Atmos., 105, 9791–9806, 2000. 6451

Dubovik, O., Holben, B., Eck, T. F., Smirnov, A., Kaufman, Y. J., King, M. D., Tanre, D., and Slutsker, I.: Variability of absorption and optical properties of key aerosol types observed in worldwide locations, J. Atmos. Sci., 59, 590–608, 2002. 6448, 6449, 6450, 6457, 6458

Dubovik, O., Sinyuk, A., Lapyonok, T., Holben, B. N., Mishchenko, M., Yang, P., Eck, T. F., Volten, H., Muñoz, O., Veihelmann, B., van der Zande, W. J., Leon, J.-F., Sorokin, M., and Slutsker,

ACPD
15, 6445–6479, 2015

I.: Application of spheroid models to account for aerosol particle nonsphericity in remote sensing of desert dust, J. Geophys. Res.-Atmos., 111, D11208, doi:10.1029/2005JD006619, 2006. 6451

Dubovik, O., Herman, M., Holdak, A., Lapyonok, T., Tanré, D., Deuzé, J. L., Ducos, F., Sinyuk, A., and Lopatin, A.: Statistically optimized inversion algorithm for enhanced retrieval of aerosol properties from spectral multi-angle polarimetric satellite observations, Atmos. Meas. Tech., 4, 975–1018, doi:10.5194/amt-4-975-2011, 2011. 6449

Eck, T., Holben, B., Reid, J., O'Neill, N., Schafer, J., Dubovik, O., Smirnov, A., Yamasoe, M., and Artaxo, P.: High aerosol optical depth biomass burning events: a comparison of optical properties for different source regions, Geophys. Res. Lett., 30, 2035, doi:10.1029/2003GL017861, 2003. 6448, 6457

Eck, T. F., Holben, B. N., Reid, J. S., Sinyuk, A., Hyer, E. J., O'Neill, N. T., Shaw, G. E., Vande Castle, J. R., Chapin, F. S., Dubovik, O., Smirnov, A., Vermote, E., Schafer, J. S., Giles, D., Slutsker, I., Sorokine, M., and Newcomb, W. W.: Optical properties of boreal region biomass burning aerosols in central Alaska and seasonal variation of aerosol optical depth at an Arctic coastal site, J. Geophys. Res.-Atmos., 114, D11201, doi:10.1029/2008JD010870, 2009. 6448, 6450, 6452, 6457, 6461

Ester, M., Kriegel, H.-P., Sander, J., and Xu, X.: A density-based algorithm for discovering clusters in large spatial databases with noise, in: Proceedings of the Second International Conference on Knowledge Discovery and Data Mining (KDD-96), edited by: Simoudis, E., Han, J., and Fayyad, U., 226–231. Menlo Park, CA: AAAI Press., 1996. 6453

Fiebig, M., Stohl, A., Wendisch, M., Eckhardt, S., and Petzold, A.: Dependence of solar radiative forcing of forest fire aerosol on ageing and state of mixture, Atmos. Chem. Phys., 3, 881–891, doi:10.5194/acp-3-881-2003, 2003. 6448

Giglio, L., Descloitres, J., Justice, C. O., and Kaufman, Y. J.: An enhanced contextual fire detection algorithm for MODIS, Remote Sens. Environ., 87, 273–282, 2003. 6452

Giles, D. M., Holben, B. N., Eck, T. F., Sinyuk, A., Smirnov, A., Slutsker, I., Dickerson, R., Thompson, A., and Schafer, J.: An analysis of AERONET aerosol absorption properties and classifications representative of aerosol source regions, J. Geophys. Res.-Atmos., 117, D17203, doi:10.1029/2012JD018127, 2012. 6449, 6450

Haywood, J., Francis, P., Dubovik, O., Glew, M., and Holben, B.: Comparison of aerosol size distributions, radiative properties, and optical depths determined by aircraft observa-

ACPD
15, 6445–6479, 2015

tions and Sun photometers during SAFARI 2000, J. Geophys. Res.-Atmos., 108, 8471, doi:10.1029/2002JD002250, 2003. 6451
Hegg, D. A., Livingston, J., Hobbs, P. V., Novakov, T., and Russell, P.: Chemical apportionment of aerosol column optical depth off the mid-Atlantic coast of the United States, J. Geophys. Res.-Atmos., 102, 25293–25303, 1997. 6460
Hobbs, P. V., Reid, J. S., Herring, J. A., Nance, J. D., and Weiss, R. E.: Particle and Trace-Gas Measurements in the Smoke from Prescribed Burns of Forest Products in the Pacific Northwest,in: Biomass Burning and Global Change, Vol. 1, edited by: Levine, J. S., 697–715, MIT Press, New York, 1006, 1996. 6448, 6460
Holben, B., Eck, T., Slutsker, I., Tanre, D., Buis, J., Setzer, A., Vermote, E., Reagan, J., Kaufman, Y., Nakajima, T., Lavenu, F., Jankowiak, I., and Smirnov, A.: AERONET a federated instrument network and data archive for aerosol characterization, Remote Sens. Environ., 66, 1–16, 1998. 6449
Holben, B., Eck, T., Slutsker, I., Smirnov, A., Sinyuk, A., Schafer, J., Giles, D., and Dubovik, O.: AERONET's version 2.0 quality assurance criteria, in: Asia-Pacific Remote Sensing Symposium, Goa, India, 13–17 November 2006, 6408, 2006. 6451
Holzer-Popp, T., de Leeuw, G., Griesfeller, J., Martynenko, D., Klüser, L., Bevan, S., Davies, W., Ducos, F., Deuzé, J. L., Graigner, R. G., Heckel, A., von Hoyningen-Hüne, W., Kolmonen, P., Litvinov, P., North, P., Poulsen, C. A., Ramon, D., Siddans, R., Sogacheva, L., Tanre, D., Thomas, G. E., Vountas, M., Descloitres, J., Griesfeller, J., Kinne, S., Schulz, M., and Pinnock, S.: Aerosol retrieval experiments in the ESA Aerosol_cci project, Atmos. Meas. Tech., 6, 1919–1957, doi:10.5194/amt-6-1919-2013, 2013. 6449, 6454
Jacobson, M. Z.: Strong radiative heating due to the mixing state of black carbon in atmospheric aerosols, Nature, 409, 695–697, 2001. 6448
Janhäll, S., Andreae, M. O., and Pöschl, U.: Biomass burning aerosol emissions from vegetation fires: particle number and mass emission factors and size distributions, Atmos. Chem. Phys., 10, 1427–1439, doi:10.5194/acp-10-1427-2010, 2010. 6447, 6448
Johnson, B., Christopher, S., Haywood, J., Osborne, S., McFarlane, S., Hsu, C., Salustro, C., and Kahn, R.: Measurements of aerosol properties from aircraft, satellite and ground-based remote sensing: a case-study from the Dust and Biomass-burning Experiment (DABEX), Q. J. Roy. Meteor. Soc., 135, 922–934, 2009. 6451

ACPD
15, 6445–6479, 2015

Johnston, F. H., Henderson, S. B., Chen, Y., Randerson, J. T., Marlier, M., DeFries, R. S., Kinney, P., Bowman, D. M., and Brauer, M.: Estimated global mortality attributable to smoke from landscape fires, Environ. Health Persp., 120, 695–701, 2012. 6447

Kahn, R. A., Chen, Y., Nelson, D. L., Leung, F.-Y., Li, Q., Diner, D. J., and Logan, J. A.: Wildfire smoke injection heights: two perspectives from space, Geophys. Res. Lett., 35, L04809, doi:10.1029/2007GL032165, 2008. 6448

Kahn, R. A., Nelson, D. L., Garay, M. J., Levy, R. C., Bull, M. A., Diner, D. J., Martonchik, J. V., Paradise, S. R., Hansen, E. G., and Remer, L. A.: MISR aerosol product attributes and statistical comparisons with MODIS, IEEE T. Geosci. Remote, 47, 4095–4114, 2009. 6449

Kasischke, E. S., Williams, D., and Barry, D.: Analysis of the patterns of large fires in the boreal forest region of Alaska, Int. J. Wildland Fire, 11, 131–144, 2002. 6452

Kaufman, Y. J., Hobbs, P. V., Kirchhoff, V. W. J. H., Artaxo, P., Remer, L. A., Holben, B. N., King, M. D., Ward, D. E., Prins, E. M., Longo, K. M., Mattos, L. F., Nobre, C. A., Spinhirne, J. D., Ji, Q., Thompson, A. M., Gleason, J. F., Christopher, S. A., and Tsay, S.-C.: Smoke, Clouds, and Radiation-Brazil (SCAR-B) experiment, J. Geophys. Res.-Atmos., 103, 31783–31808, 1998a. 6459, 6461, 6463

Kaufman, Y. J. and Tanre, D.: Algorithm for remote sensing of tropospheric aerosol from MODIS, NASA MODIS Algorithm Theoretical Basis Document, Goddard Space Flight Center,Greenbelt, Md, 85 pp., 1998b. 6454

Kinne, S., Lohmann, U., Feichter, J., Schulz, M., Timmreck, C., Ghan, S., Easter, R., Chin, M., Ginoux, P., Takemura, T., Tegen, I., Koch, D., Herzog, M., Penner, J., Pitari, G., Holben, B., Eck, T., Smirnov, A., Dubovik, O., Slutsker, I., Tanre, D., Torres, O., Mishchenko, M., Geogdzhayev, I., Chu, D. A., and Kaufman, Y.: Monthly averages of aerosol properties: a global comparison among models, satellite data, and AERONET ground data, J. Geophys. Res.-Atmos., 108, 4634, doi:10.1029/2001JD001253, 2003. 6449

Koch, D., Schulz, M., Kinne, S., McNaughton, C., Spackman, J. R., Balkanski, Y., Bauer, S., Berntsen, T., Bond, T. C., Boucher, O., Chin, M., Clarke, A., De Luca, N., Dentener, F., Diehl, T., Dubovik, O., Easter, R., Fahey, D. W., Feichter, J., Fillmore, D., Freitag, S., Ghan, S., Ginoux, P., Gong, S., Horowitz, L., Iversen, T., Kirkevåg, A., Klimont, Z., Kondo, Y., Krol, M., Liu, X., Miller, R., Montanaro, V., Moteki, N., Myhre, G., Penner, J. E., Perlwitz, J., Pitari, G., Reddy, S., Sahu, L., Sakamoto, H., Schuster, G., Schwarz, J. P., Seland, Ø., Stier, P., Takegawa, N., Takemura, T., Textor, C., van Aardenne, J. A., and Zhao, Y.: Evaluation of

ACPD
15, 6445–6479, 2015

black carbon estimations in global aerosol models, Atmos. Chem. Phys., 9, 9001–9026, doi:10.5194/acp-9-9001-2009, 2009. 6447

Kokhanovsky, A. A., Deuzé, J. L., Diner, D. J., Dubovik, O., Ducos, F., Emde, C., Garay, M. J., Grainger, R. G., Heckel, A., Herman, M., Katsev, I. L., Keller, J., Levy, R., North, P. R. J., Prikhach, A. S., Rozanov, V. V., Sayer, A. M., Ota, Y., Tanré, D., Thomas, G. E., and Zege, E. P.: The inter-comparison of major satellite aerosol retrieval algorithms using simulated intensity and polarization characteristics of reflected light, Atmos. Meas. Tech., 3, 909–932, doi:10.5194/amt-3-909-2010, 2010. 6449

Langmann, B., Duncan, B., Textor, C., Trentmann, J., and van der Werf, G. R.: Vegetation fire emissions and their impact on air pollution and climate, Atmos. Environ., 43, 107–116, 2009. 6447

Lee, J., Kim, J., Song, C., Kim, S., Chun, Y., Sohn, B., and Holben, B.: Characteristics of aerosol types from AERONET sunphotometer measurements, Atmos. Environ., 44, 3110–3117, 2010. 6449

Levy, R. C., Remer, L. A., Tanre, D., Mattoo, S., and Kaufman, Y. J.: Algorithm for Remote Sensing of Tropospheric Aerosol over Dark Targets from MODIS: Collections 005 and 051: Revision 2; Feb 2009, available at: http://modis-atmos.gsfc.nasa.gov/_docs/ATBD_MOD04_C005_rev2.pdf (last access: 24 February 2015), 2009. 6454

Levy, R. C., Remer, L. A., Kleidman, R. G., Mattoo, S., Ichoku, C., Kahn, R., and Eck, T. F.: Global evaluation of the Collection 5 MODIS dark-target aerosol products over land, Atmos. Chem. Phys., 10, 10399–10420, doi:10.5194/acp-10-10399-2010, 2010. 6454

Loveland, T. and Belward, A.: The IGBP-DIS global 1km land cover data set, DISCover: first results, Int. J. Remote Sens., 18, 3289–3295, 1997. 6453, 6473

Myhre, G., Samset, B. H., Schulz, M., Balkanski, Y., Bauer, S., Berntsen, T. K., Bian, H., Bellouin, N., Chin, M., Diehl, T., Easter, R. C., Feichter, J., Ghan, S. J., Hauglustaine, D., Iversen, T., Kinne, S., Kirkevåg, A., Lamarque, J.-F., Lin, G., Liu, X., Lund, M. T., Luo, G., Ma, X., van Noije, T., Penner, J. E., Rasch, P. J., Ruiz, A., Seland, Ø., Skeie, R. B., Stier, P., Takemura, T., Tsigaridis, K., Wang, P., Wang, Z., Xu, L., Yu, H., Yu, F., Yoon, J.-H., Zhang, K., Zhang, H., and Zhou, C.: Radiative forcing of the direct aerosol effect from AeroCom Phase II simulations, Atmos. Chem. Phys., 13, 1853–1877, doi:10.5194/acp-13-1853-2013, 2013. 6447

ACPD
15, 6445–6479, 2015

Nakajima, T., Higurashi, A., Takeuchi, N., and Herman, J. R.: Satellite and ground-based study of optical properties of 1997 Indonesian forest fire aerosols, Geophys. Res. Lett., 26, 2421–2424, 1999. 6448

North, P. R.: Estimation of aerosol opacity and land surface bidirectional reflectance from ATSR-2 dual-angle imagery: operational method and validation, J. Geophys. Res.-Atmos., 107, AAC–4-1, doi:10.1029/2000JD000207, 2002. 6454

O'Neill, N., Eck, T., Holben, B., Smirnov, A., Royer, A., and Li, Z.: Optical properties of boreal forest fire smoke derived from Sun photometry, J. Geophys. Res.-Atmos., 107, AAC–6-1, doi:10.1029/2001JD000877, 2002. 6448, 6449

Reid, J. S. and Hobbs, P. V.: Physical and optical properties of young smoke from individual biomass fires in Brazil, J. Geophys. Res.-Atmos., 103, 32013–32030, 1998. 6448, 6457

Reid, J. S., Hobbs, P. V., Ferek, R. J., Blake, D. R., Martins, J. V., Dunlap, M. R., and Liousse, C.: Physical, chemical, and optical properties of regional hazes dominated by smoke in Brazil, J. Geophys. Res.-Atmos., 103, 32059–32080, 1998. 6448, 6450, 6459, 6461, 6462, 6463

Reid, J. S., Koppmann, R., Eck, T. F., and Eleuterio, D. P.: A review of biomass burning emissions part II: intensive physical properties of biomass burning particles, Atmos. Chem. Phys., 5, 799–825, doi:10.5194/acp-5-799-2005, 2005a. 6447, 6448, 6457, 6458

Reid, J. S., Eck, T. F., Christopher, S. A., Koppmann, R., Dubovik, O., Eleuterio, D. P., Holben, B. N., Reid, E. A., and Zhang, J.: A review of biomass burning emissions part III: intensive optical properties of biomass burning particles, Atmos. Chem. Phys., 5, 827–849, doi:10.5194/acp-5-827-2005, 2005b. 6447, 6458, 6461

Sayer, A. M., Hsu, N. C., Eck, T. F., Smirnov, A., and Holben, B. N.: AERONET-based models of smoke-dominated aerosol near source regions and transported over oceans, and implications for satellite retrievals of aerosol optical depth, Atmos. Chem. Phys., 14, 11493–11523, doi:10.5194/acp-14-11493-2014, 2014. 6450, 6462

Shiraiwa, M., Kondo, Y., Iwamoto, T., and Kita, K.: Amplification of light absorption of black carbon by organic coating, Aerosol Sci. Tech., 44, 46–54, 2010. 6448

Smirnov, A., Holben, B., Dubovik, O., O'Neill, N., Remer, L., Eck, T., Slutsker, I., and Savoie, D.: Measurement of atmospheric optical parameters on US Atlantic coast sites, ships, and Bermuda during TARFOX, J. Geophys. Res.-Atmos., 105, 9887–9901, 2000. 6460

Stocks, B. J., Mason, J. A., Todd, J. B., Bosch, E. M., Wotton, B. M., Amiro, B. D., Flannigan, M. D., Hirsch, K. G., Logan, K. A., Martell, D. L., and Skinner, W. R.: Large forest fires in Canada, 1959–1997, J. Geophys. Res.-Atmos., 107, 8149, doi:10.1029/2001JD000484, 2002. 6452

ACPD
15, 6445–6479, 2015

Torres, O., Tanskanen, A., Veihelmann, B., Ahn, C., Braak, R., Bhartia, P. K., Veefkind, P., and Levelt, P.: Aerosols and surface UV products from Ozone Monitoring Instrument observations: an overview, J. Geophys. Res.-Atmos., 112, D24S47, doi:10.1029/2007JD008809, 2007. 6449

Val Martin, M., Logan, J. A., Kahn, R. A., Leung, F.-Y., Nelson, D. L., and Diner, D. J.: Smoke injection heights from fires in North America: analysis of 5 years of satellite observations, Atmos. Chem. Phys., 10, 1491–1510, doi:10.5194/acp-10-1491-2010, 2010. 6448

van der Werf, G. R., Randerson, J. T., Giglio, L., Collatz, G. J., Mu, M., Kasibhatla, P. S., Morton, D. C., DeFries, R. S., Jin, Y., and van Leeuwen, T. T.: Global fire emissions and the contribution of deforestation, savanna, forest, agricultural, and peat fires (1997–2009), Atmos. Chem. Phys., 10, 11707–11735, doi:10.5194/acp-10-11707-2010, 2010. 6447

ACPD
15, 6445–6479, 2015

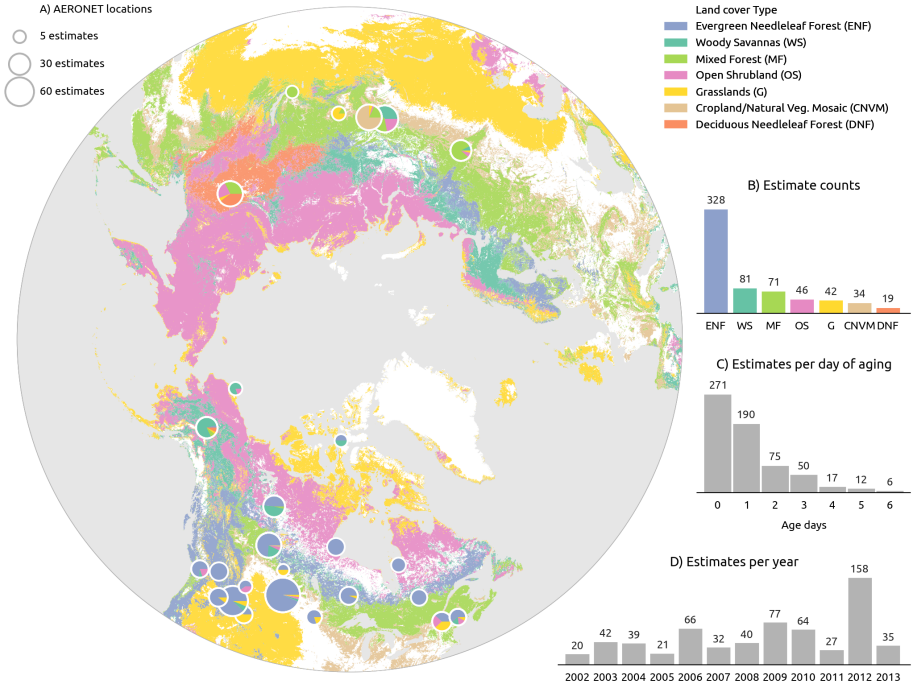

Figure 1. (a) Study area, land cover types examined and locations of AERONET stations used. MODIS MCD12C1 land cover data products were employed with classes defined by the International Geosphere Biosphere Programme classification system (Loveland and Belward, 1997). Pie charts inside the circles indicate the origin land cover type of plumes observed at the AERONET stations as estimated in this study. **(b–d)** show total estimate counts per source land cover type, smoke age per day of ageing and estimate number for each year.

ACPD
15, 6445–6479, 2015

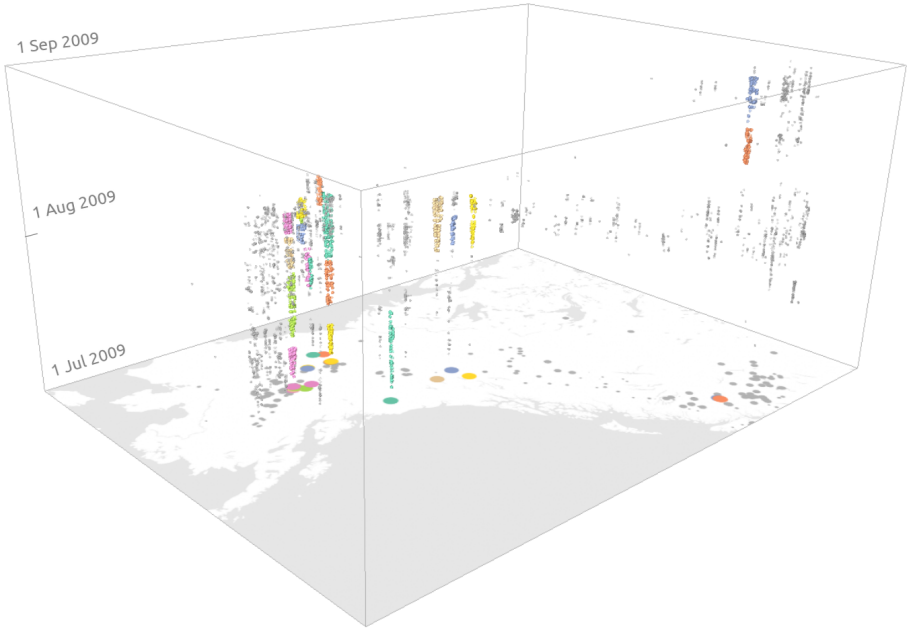

Figure 2. An illustration of the DBSCAN fire pixel segmentation method. Individual MODIS active fires in north-west Canada, Alaska and the north-western USA observed during July–August (vertical axis) in 2009. Colours show separate, large fire objects used in the analysis. Grey fire pixels were removed as described in Sect. 2.2.1.

ACPD
15, 6445–6479, 2015

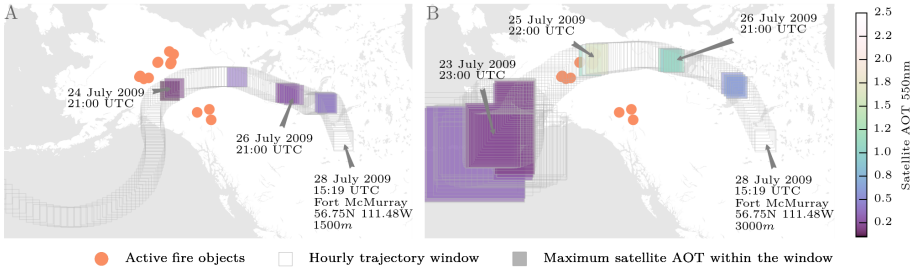

Figure 3. Two 7 day back trajectories ending at Fort McMurray AERONET station and coinciding fire and Satellite AOT observations. **(a)** trajectory ending at 1500 m altitude does pass close to active fire objects but satellite AOT remains low. **(b)** trajectory ending at 3000 m altitude passes close to the fire objects followed by a sudden increase in observed AOT, indicating the source and age for the AERONET smoke observation.

ACPD
15, 6445–6479, 2015

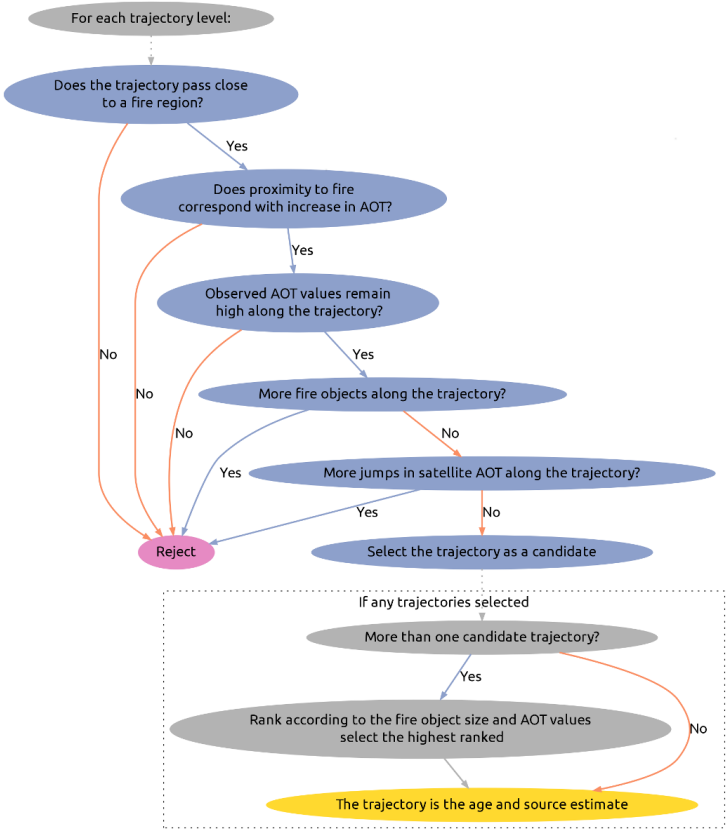

Figure 4. The decision tree used to identify potential smoke source and age. For every AERONET observation back trajectories arriving at different altitudes are tested against the conditions defined in the main part of the decision tree. Any trajectories identified as potential candidates are ranked (lower part of the diagram), identifying a single source and age estimate for the AERONET observation.

ACPD
15, 6445–6479, 2015

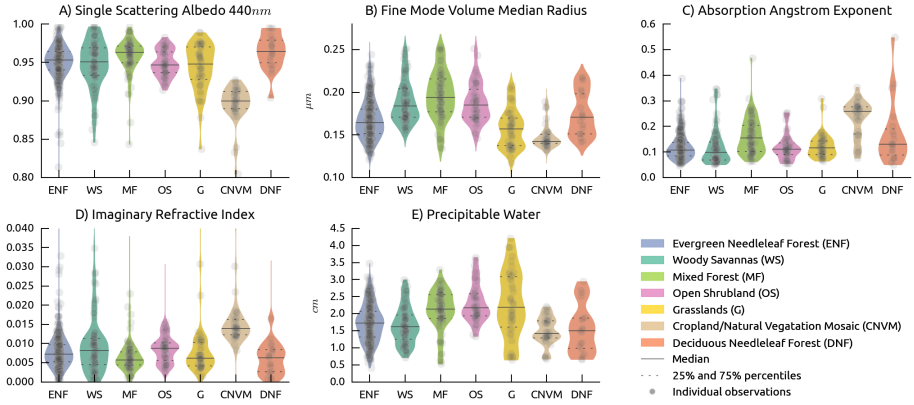

Figure 5. Optical and microphysical properties of smoke attributed to different land cover types. Coloured areas indicate kernel density estimates.

ACPD
15, 6445–6479, 2015

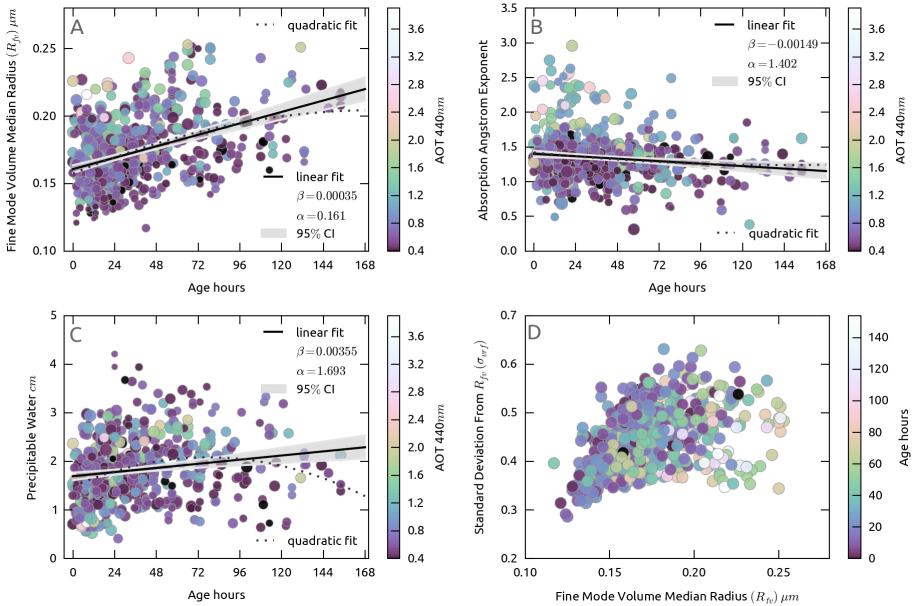

Figure 6. Relationships between estimated age and AERONET retrieved plume properties. **(a)** fine mode volume median radius, **(b)** Absorption Angstrom Exponent, **(c)** precipitable water content, and **(d)** fine mode volume radius against fine mode volume radius spread and smoke age estimates. Marker size in **(a–c)** indicates the SD from fine mode volume radius.

ACPD
15, 6445–6479, 2015

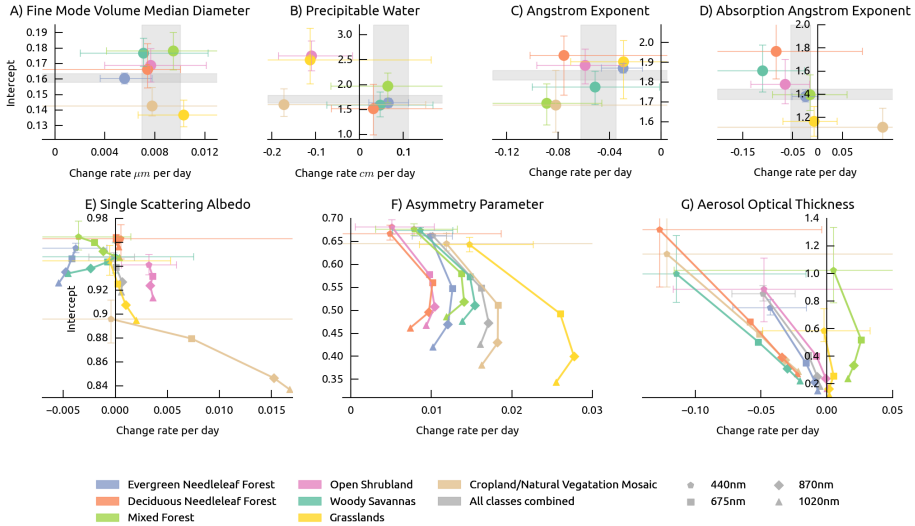

Figure 7. Linear regression coefficients as change rates and initial smoke plume optical and microphysical properties estimated for different land cover types **(a–d)** and for different land cover types and different wavelengths **(e–g)**. Shaded areas in top panels indicate 95 % CI of all data fits. Error bars representing 95 % CI in **(e–g)** are shown only for 440 nm for clarity.

ACPD
15, 6445–6479, 2015